



Contents lists available at ScienceDirect

**Journal of Biomechanics**journal homepage: www.elsevier.com/locate/jbiomech
www.JBiomech.com**Prevalent role of porosity and osteonal area over mineralization heterogeneity in the fracture toughness of human cortical bone**Mathilde Granke ^{a,b,c}, Alexander J. Makowski ^{a,b,c,d}, Sasidhar Uppuganti ^{a,b},
Jeffry S. Nyman ^{a,b,c,d,*}^a Department of Orthopaedics Surgery & Rehabilitation, Vanderbilt University Medical Center, Nashville, TN 37232, United States^b Center for Bone Biology, Vanderbilt University Medical Center, Nashville, TN 37232, United States^c Department of Veterans Affairs, Tennessee Valley Healthcare System, Nashville, TN 37212, United States^d Department of Biomedical Engineering, Vanderbilt University, Nashville, TN 37232, United States**ARTICLE INFO****Article history:**

Accepted 7 June 2016

Keywords:

Fracture toughness

Heterogeneity

Mineralization

Porosity

Microstructure

ABSTRACT

Changes in the distribution of bone mineralization occurring with aging, disease, or treatment have prompted concerns that alterations in mineralization heterogeneity may affect the fracture resistance of bone. Yet, so far, studies assessing bone from hip fracture cases and fracture-free women have not reached a consensus on how heterogeneity in tissue mineralization relates to skeletal fragility. Owing to the multifactorial nature of toughening mechanisms occurring in bone, we assessed the relative contribution of heterogeneity in mineralization to fracture resistance with respect to age, porosity, and area fraction of osteonal tissue. The latter parameters were extracted from quantitative backscattered electron imaging of human cortical bone sections following *R*-curve tests of single-edge notched beam specimens to determine fracture toughness properties. Microstructural heterogeneity was determined as the width of the mineral distribution (bulk) and as the sill of the variogram (local). In univariate analyses of measures from 62 human donors (21 to 101 years), local but not bulk heterogeneity as well as pore clustering negatively correlated with fracture toughness properties. With age as covariate, heterogeneity was a significant predictor of crack initiation, though local had a stronger negative contribution than bulk. When considering all potential covariates, age, cortical porosity and area fraction of osteons explained up to 50% of the variance in bone's crack initiation toughness. However, including heterogeneity in mineralization did not improve upon this prediction. The findings of the present work stress the necessity to account for porosity and microstructure when evaluating the potential of matrix-related features to affect skeletal fragility.

Published by Elsevier Ltd.

1. Introduction

The fracture resistance of bone does not solely depend on the quantity of bone, or bone mineral density, but also on the integrity of the bone tissue (Donnelly et al., 2014). In particular, owing to its hierarchical organization, bone is able to resist fracture through the combination of multiple toughening mechanisms that interact at several length scales. For example, interfibrillar sliding at the nanoscale allows the mineralized collagen fibrils to deform without failing, while osteons on the order of hundreds of microns create natural barriers to the propagation of cracks through bone

tissue (O'Brien et al., 2003; Ural and Vashishth, 2014). With aging and disease progression, changes can occur at any of the hierarchical levels of organization, thereby lowering the fracture resistance of bone (e.g., accumulation of non-enzymatic collagen crosslinks impeding interfibrillar sliding). Complicating the clinical assessment of fracture resistance or fracture risk, heterogeneity exists at the multiple length scales of organization, but not all heterogeneity may significantly contribute to the age-related loss of fracture resistance.

Investigations of fracture processes in material science indicate that microstructural heterogeneity (i.e., the spatial variation of compositional properties in a material) improves resistance to fracture: crack propagation is straight in a homogenous material with less energy dissipation while it is tortuous deflecting at interfaces in a heterogeneous material, thereby requiring more energy to grow (Dimas et al., 2014; Hossain et al., 2014). Changes

* Corresponding author at: Department of Orthopaedics Surgery & Rehabilitation, Vanderbilt University Medical, Medical Center East, South Tower, Suite 4200, Nashville, TN 37232, United States. Fax: +1 615 936 0117.

E-mail address: jeffry.s.nyman@vanderbilt.edu (J.S. Nyman).

in bone metabolism associated with diseases or drug treatment are known to significantly affect the distribution of bone mineralization at the micron length scale (Roschger et al., 2008). In this context, a loss in heterogeneity in mineralization has been posited as a possible factor contributing to an increase in fracture risk (Ettinger et al., 2013). However, in the current literature, there is a lack of consensus on how heterogeneity in tissue mineralization relates to skeletal fragility. Indeed, heterogeneity in mineralization at the micro-structural level was found either to be greater (Bousson et al., 2011) or lower (Gourion-Arsiquaud et al., 2013; Milovanovic et al., 2014) in treatment naïve, hip fracture cases compared to fracture-free women. The inconsistency of these results highlights the need to account for other contributing factors to conclusively state that bone fragility is directly related to the distribution of tissue mineralization.

Among the factors that contribute to skeletal fragility, vascular porosity is greater in patients with a history of fracture compared to non-fracture controls (Ahmed et al., 2015; Bala et al., 2014; Bell et al., 1999; Milovanovic et al., 2014; Shigdel et al., 2015) or in bone specimens with lower fracture toughness properties, as determined from mechanical tests of cadaveric tissue (Granke et al., 2015; Yeni et al., 1997). Moreover, image analysis of bone cross-sections of the femoral neck suggests that greater cortical porosity in fragile bone may result from the merging of spatially clustered remodeling osteons (Bell et al., 2000; Jordan et al., 2000). Therefore, not only the extent but also the spatial distribution of porosity may decrease the fracture resistance of bone, a phenomenon described for porous media (Bilger et al., 2005).

To date, the question of whether heterogeneity mineralization affects bone's resistance to fracture remains undetermined for two reasons. First, published data is confined to comparing tissue composition between fracture and control cases, but to date, no studies have attempted to relate heterogeneity in mineralization and the mechanical properties of cortical bone. Second, most studies investigating associations between tissue composition and fracture status or risk do not adjust for other microstructural features (i.e., porosity or bone volume fraction). Given the possible contribution of age, porosity, and tissue microstructure to skeletal fragility, we aimed to determine whether microstructural heterogeneity in mineralization significantly explains bone's ability to resist fracture after adjusting for these factors. To address this, we analyzed cross-sections of human cortical bone specimens for which fracture toughness properties had been previously determined (Granke et al., 2015). Upon imaging these cross-sections by quantitative backscattered electron imaging (qBEI), image processing techniques quantified lacunar and vascular porosities, pore clustering, population and local heterogeneity in mineralization, as well as area fraction of osteonal tissue.

2. Material and methods

The preparation of the mechanical specimens and measurement methods are extensively described in Granke et al. (2015) and briefly summarized herein. Femurs from sixty-two human donors (30 male, age = 63.5 ± 23.7 [21–98] years and 32 female, age = 64.4 ± 21.3 [23–101] years) were obtained from the Musculoskeletal Transplant Foundation (Edison, NJ), the Vanderbilt Donor Program (Nashville, TN), and the National Disease Research Interchange (Philadelphia, PA) and stored fresh-frozen. Single-sedge notched beam (SENB) specimens (span \times thickness \times width $\sim 20 \times 2.5 \times 5.0 \text{ mm}^3$) were machined from the lateral quadrant of each femoral mid-shaft ($N=62$). After imaging the notched region with micro-computed tomography (μCT) at a $5 \mu\text{m}$ voxel size (Granke et al., 2015) to determine vascular porosity, a progressive, loading/partial unloading/reloading scheme in a three-point bending configuration was used to initiate and propagate a crack from the micro-notch through the cortical bone such that crack extension was perpendicular to the osteonal direction. A non-linear fracture mechanics approach based on the analysis of the resulting R -curve (J -integral vs. crack length) provided the resistance (elastic plus plastic contributions) to initiate (K_{init}) and propagate (K_{grow}) a crack from the notch as well as the energy dissipated during fracture (J) (ASTM Standard E1820-15a, 2015).

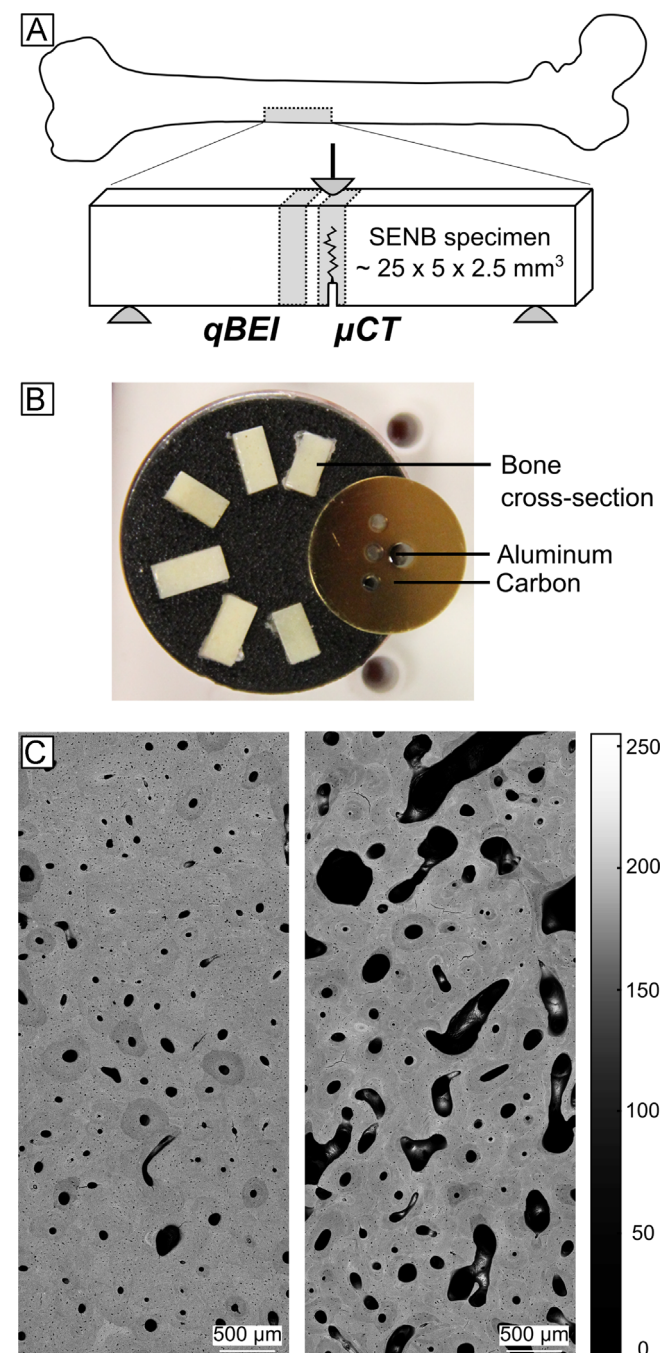


Fig. 1. Study design. (A) Single-edge notch beam specimens were machined from the femoral mid-shaft. The notch region was scanned with μCT to image porosity prior to mechanical testing. (B) Following fracture toughness testing, a cross-section was cut close to the fracture line, polished, and mounted on a stub with standard materials for calibration. (C) qBEI images (in gray levels) of bone from young (23-year-old, left) and old (96-year-old, right) donors.

K_{grow} could not be calculated for specimens that exhibit highly brittle behavior, which was the case for 11 specimens out of 62. Following mechanical testing, the specimens were stored in phosphate-buffered saline at -20°C until the next phase of the experimental protocol.

2.1. Quantitative backscattered electron imaging (qBEI)

2.1.1. Specimens preparation and image acquisition

A cross-section ($\sim 2.5 \text{ mm} \times 4.5 \text{ mm}$) was cut adjacent to the fracture line (Fig. 1), ground on successive grits (1200–4000) of wet silicon carbide paper, and polished on synthetic cloth with $0.05 \mu\text{m}$ aluminum oxide suspension (MasterPrep, Buehler, Lake Bluff, IL). Upon drying for several days in a vacuum desiccator at room

temperature, the samples were mounted on aluminum stubs with double-sided carbon tape together with pure aluminum and carbon standards for calibration (EMS, Hatfield PA) (Fig. 1). The surface of the specimen was imaged by qBEI using a Quanta FEG 250 ESEM (FEI Company, Hillsboro, Oregon, USA) equipped with a low-voltage, high-contrast backscattered electron detector. Digital images from the bone cross-section and calibration materials were acquired using the same settings (high vacuum mode, acceleration voltage of 20 kV, working distance of 15 mm, scan speed of 100 s/frame). Contrast and brightness were adjusted so that the mean gray levels of the backscattered signals from carbon and aluminum reached 25 and 225, respectively. In order to cover the entire surface of the cross-section, four to six images ($2 \times 2.5 \text{ mm}^2$) were collected at $50 \times$ magnification with a $1.2 \mu\text{m}$ pixel resolution, merged to a single image using Photoshop[®] CS6 (Adobe Systems Inc., San Jose, CA, USA), and Gauss-filtered ($\sigma=1$) (Fig. 1). Although the specimens were not carbon-coated, electron charging did not build up as demonstrated by imaging the same bone surface repeatedly over the course of 15 min (Supplementary Fig. 1) and by imaging the same specimen before and after carbon coating (Supplementary Fig. 2). All the following post-processing analyses were implemented in MATLAB[®] (The Mathworks Inc., Natick, MA, USA).

2.1.2. Porosity analysis

A semi-automated procedure was used to segment the pores from the bony matrix (Fig. 2A). A porosity mask was first created using Otsu's method (Otsu, 1979). Any surface contaminants (e.g., dust particles) and large cracks were manually removed from the porosity mask using Photoshop CS6 (Adobe Systems, Inc., San Jose, CA). Pores with an area larger than $100 \mu\text{m}^2$ were assigned to vascular porosity (including Haversian canals, Volkmann's canals, resorption cavities) or to lacunar porosity otherwise (Fig. 2B).

The heterogeneity in the spatial distribution of the vascular porosity was analyzed using Voronoi diagrams (Aurenhammer, 1991). The sides of the Voronoi polygons are located at mid-distance from neighboring pores (Fig. 2C). The area of each polygon was determined without excluding the pore area (black region in Fig. 2C). High coefficient of variation for the individual areas of the Voronoi polygons ($VORcv$) indicates a heterogeneous, clustered distribution of pores.

2.1.3. Mineralization heterogeneity

Given that the backscattered signal intensity is proportional to the average atomic number of a material, the mineral phase essentially dictates the qBEI intensity. Histograms of the gray-levels in the qBEI images provided the most frequently occurring gray value ($BSEpeak$) and the width at half-maximum ($BSEwidth$) describing the variation in degree of mineralization over the cross-section ($\sim 10 \text{ mm}^2$) (Fig. 3B).

The width of the histogram does not inform on the clustering of the heterogeneities (Supplementary Fig. 3). Therefore, an additional analysis involved computing experimental variograms, which were used to describe the local inhomogeneity of tissue mineralization. Descriptions of calculating variograms can be found in previous bone studies that described the inhomogeneity in tissue elastic

properties from maps of nanoindentation modulus (Dong et al., 2010) and the inhomogeneity in areal bone mineral density maps from hip scans by dual-energy X-ray absorptiometry (Dong et al., 2015). In the present study, an isotropic variogram of the qBEI image was built by computing $\gamma(h)$, the mean squared gray-level differences between pixels separated by a distance h spanning from 1 to $250 \mu\text{m}$. Upon fitting the experimental variogram with an exponential function,

$$\gamma(h) = c_0 + c(1 - e^{-\frac{h}{2l}}) \quad (1)$$

The asymptote of the variogram ($c+c_0$) or *sill* provided a measure of the semivariance in mineralization over a length scale of $250 \mu\text{m}$ (Fig. 3C). This length scale was chosen because it is small enough to represent the variance in mineralization at a local scale (i.e., the scale of an osteon) and it is large enough to ensure that pixels would not be auto-correlated (i.e., once the variogram levels off).

2.1.4. Microstructure analysis

Based on differences in gray levels, osteonal and interstitial tissues were manually segmented within a sub-region ($1.5 \text{ mm} \times 1.5 \text{ mm}$) at the center of each qBEI image (Fig. 4B) using an interactive tablet monitor (Wacom Technology Co., Vancouver, WA). Manual segmentation is commonly used to distinguish osteonal from interstitial tissue (Bernhard et al., 2013; Tommasini et al., 2008; Wachter et al., 2002; Wang et al., 2015) and increasing the image contrast for this step made the segmentation unambiguous. Area fraction of osteonal tissue (*OstAr*) with respect to the total area of the sub-region was computed for each sub-region. *BSEpeak* was computed for both the distribution of osteonal and interstitial tissue, respectively. Contrast in mineralization in this sub-region was evaluated as the ratio of the interstitial *BSEpeak* to the osteonal *BSEpeak* (*IOratio*).

2.2. Statistical analysis

In a preliminary analysis, we verified that the pores examined with qBEI from neighboring cross-sections were representative of the pores within the region where the crack actually propagated (a few millimeters away in the osteon direction, Fig. 1). The vascular porosity derived from qBEI images (*VasPor*) was therefore compared to the vascular porosity of the notched region imaged with μ CT (*Ct.Po*) using the equation and correlation coefficient of the linear fit between these two quantities.

Upon running multiple linear regressions with age and gender as covariates on all parameters reported (i.e. including properties related to fracture toughness, porosity, mineralization, and microstructure), gender was only significant for K_{init} (Supplementary Table 1). Further analysis revealed that this association between gender and K_{init} was driven by two particular specimens as the *p*-value of gender was greater than 0.082 after excluding these donors ($N=60$ instead of $N=62$). Therefore, age but not gender was included as a covariate in subsequent regression analyses.

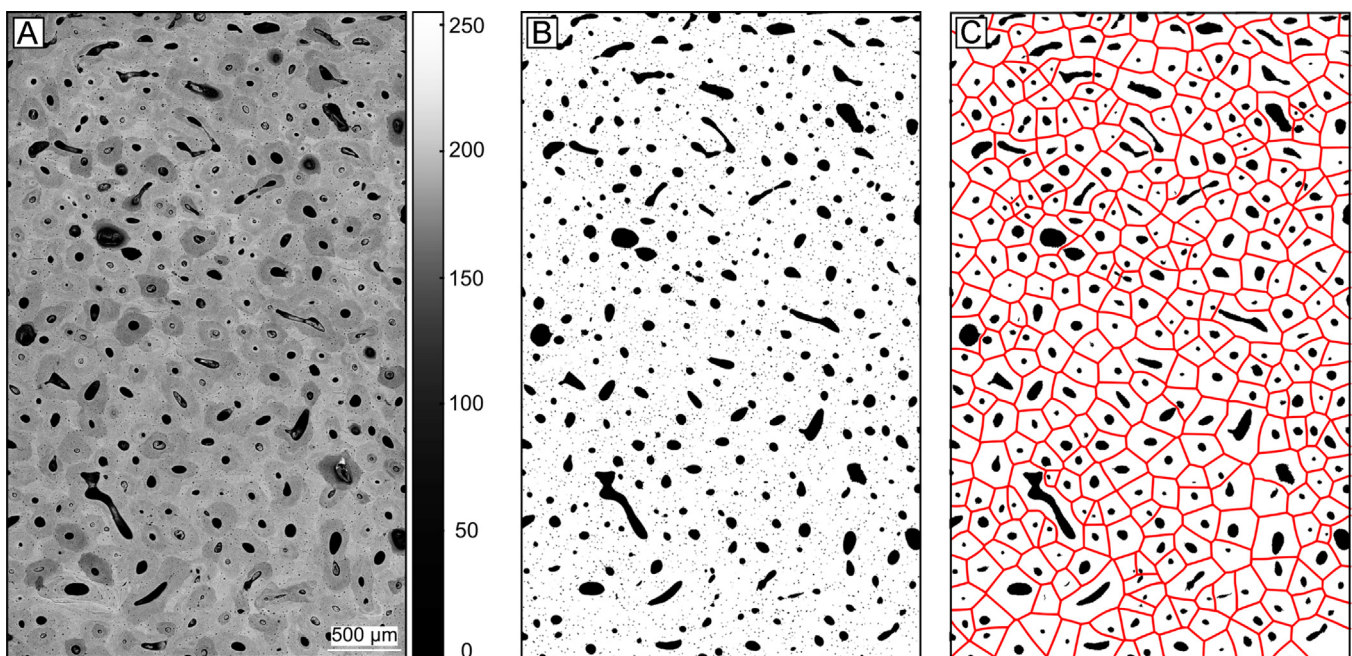


Fig. 2. Characterization of cortical porosity from qBEI images. (A) Original image from a 47 years old female donor. (B) Porosity mask: black pixels include vascular and lacunar porosity. (C) Voronoi diagrams (red) are used to quantify the spatial distribution of vascular porosity. (For interpretation of the references to color in this figure legend, the reader is referred to the web version of this article.)

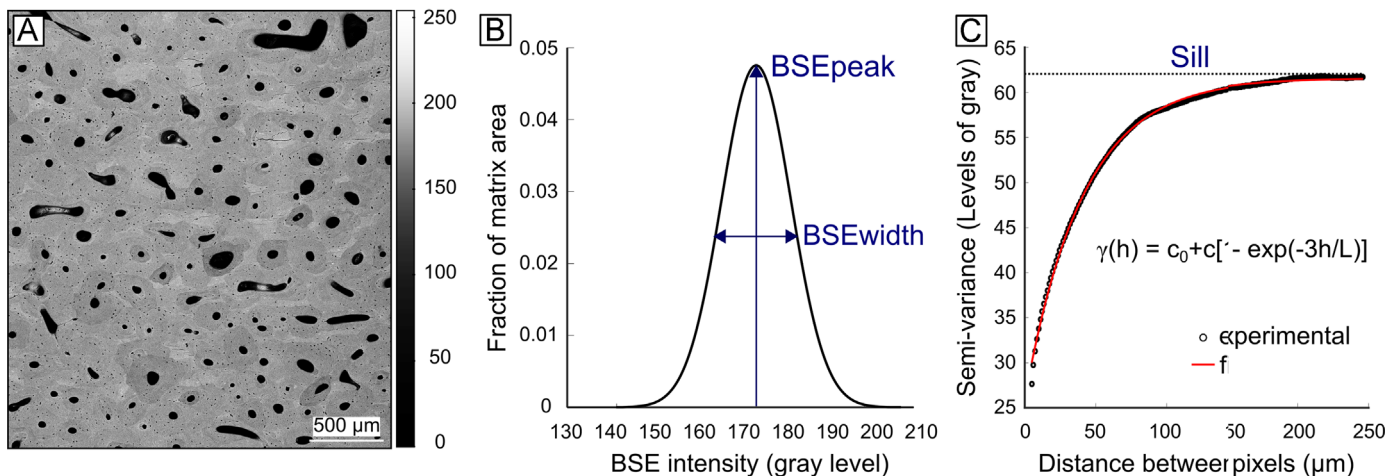


Fig. 3. Characterization of the distribution of mineralization from qBEI images. (A) Original image from a 24-year-old male donor. (B) Histogram of gray-levels in the qBEI images provides *BSEpeak*, the most frequent gray value, and *BSEwidth*, the width of the distribution, a measure of the overall heterogeneity in mineralization at the scale of the sample. (C) Experimental variogram describes the local heterogeneity in mineralization over a fixed length scale of 250 μm .

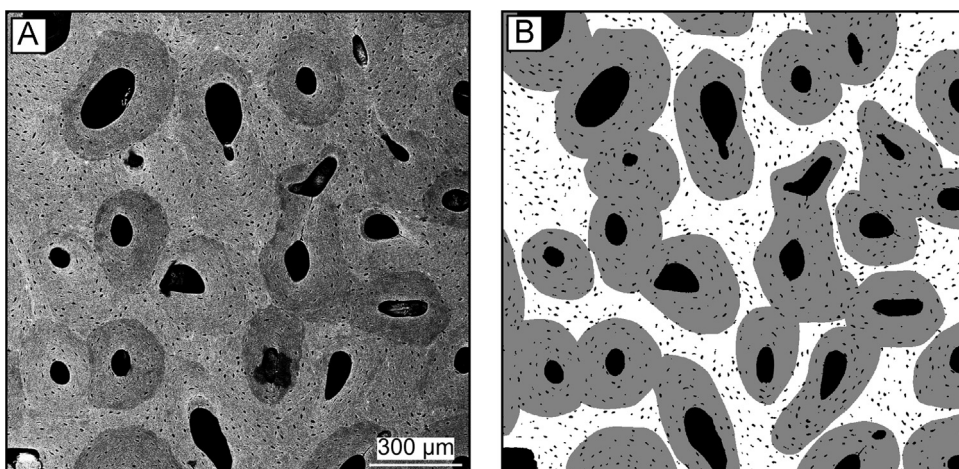


Fig. 4. A sub-region ($1.5 \times 1.5 \text{ mm}^2$) was obtained from the center of the qBEI image. (A) Enhancing the contrast of the qBEI image facilitated the visualization of the boundaries between osteonal and interstitial tissues based on gray levels. (B) Resulting segmentation distinguished between pores (black), osteonal (gray) and interstitial (white) tissue.

Table 1

Significant Pearson's correlation coefficients and corresponding *p*-values calculated from bootstrapped data.

	Porosity			Mineralization				Microstructure	
	Age	Lacunar porosity (<i>LacPor</i>)	Vascular porosity (<i>VasPor</i>)	Pore clustering (<i>VORcv</i>)	Degree of mineralization (<i>BSEpeak</i>)	Bulk heterogeneity (<i>BSEwidth</i>)	Local heterogeneity (<i>sill</i>)	Inters./Osteon heterogeneity (<i>IOratio</i>)	Osteon area fraction (<i>OstAr</i>)
Age	–	–0.43 0.002	0.33 0.039	0.39 0.004	ns ^a 0.346	–0.27 0.073	ns 0.432	–0.35 0.011	–0.45 < 0.001
<i>K_{init}</i>	–0.48 < 0.001	0.33 0.020	–0.65 < 0.001	–0.59 < 0.001	ns 0.575	ns 0.232	–0.41 < 0.001	ns 0.890	0.44 < 0.001
<i>K_{grow}</i>	–0.41 0.010	ns 0.378	–22.4 0.063	–0.31 0.006	ns 0.144	ns 0.805	ns 0.579	ns 0.207	0.36 0.020
<i>J</i>	–0.36 0.001	0.23 0.071	–0.38 < 0.001	–0.37 < 0.001	ns 0.165	ns 0.510	–0.23 0.041	ns 0.174	0.42 < 0.001

^a ns indicates that the correlation is not statistically significant.

Statistical analyses were performed on bootstrapped data (1000 replicates) to account for the non-normality of most parameters (Shapiro-Wilk test). Pearson correlation coefficients were used to assess the linear dependence of fracture toughness parameters on potential explanatory variables related to age, porosity, mineral heterogeneity, and microstructure (Table 1). Potential predictors (age and

parameters related to porosity, mineralization, and microstructure) with weak correlations ($r < 0.55$, Supplemental Table 2) and their interactions were included as independent explanatory variables in multiple linear regressions. For each model, backward stepwise elimination was used to remove non-significant terms until obtaining a combination of variables that all significantly explained the

Table 2

Best-fit multivariate linear combinations of parameters explaining the variance in the fracture toughness of human cortical bone obtained upon running multiple linear regressions using backward stepwise elimination.

Fracture toughness property	Explanatory variables	Linear model ^{a,b}	Adj-R ² (%)
K_{init}	Age + porosity	Age ($\beta = -0.29, p = 0.004$)	VasPor ($\beta = -0.55, p < 0.001$)
	Age + porosity	Age ($\beta = -0.29, p = 0.011$)	VORcv ($\beta = -0.47, p < 0.001$)
	Age + heterogeneity	Age ($\beta = -0.56, p < 0.001$)	BSEwidth ($\beta = -0.33, p = 0.005$)
	Age + heterogeneity	Age ($\beta = -0.53, p < 0.001$)	Sill ($\beta = -0.47, p < 0.001$)
	Age + microstructure	Age ($\beta = -0.35, p = 0.006$)	OstAr ($\beta = 0.29, p = 0.004$)
	Best combination	Age ($\beta = -0.22, p = 0.047$)	VasPor ($\beta = -0.52, p < 0.001$)
	Age + porosity	Age ($\beta = -0.41, p < 0.001$)	OstAr ($\beta = 0.19, p = 0.033$)
	Age + heterogeneity	Age ($\beta = -0.41, p < 0.001$)	
	Age + microstructure	Age ($\beta = -0.41, p < 0.001$)	
	Best combination	Age ($\beta = -0.41, p < 0.001$)	
K_{grow}	Age + porosity	Age ($\beta = -0.26, p = 0.028$)	VasPor ($\beta = -0.30, p = 0.007$)
	Age + porosity	Age ($\beta = -0.25, p = 0.026$)	VORcv ($\beta = -0.27, p = 0.003$)
	Age + heterogeneity	Age ($\beta = -0.39, p < 0.001$)	Sill ($\beta = -0.28, p = 0.016$)
	Age + microstructure	OstAr ($\beta = 0.42, p < 0.001$)	
	Best combination	VasPor ($\beta = -0.28, p = 0.001$)	OstAr ($\beta = 0.34, p = 0.001$)
	Age + porosity		
	Age + heterogeneity		
	Age + microstructure		
	Best combination		
J	Age + porosity	Age ($\beta = -0.26, p = 0.028$)	VasPor ($\beta = -0.30, p = 0.007$)
	Age + porosity	Age ($\beta = -0.25, p = 0.026$)	VORcv ($\beta = -0.27, p = 0.003$)
	Age + heterogeneity	Age ($\beta = -0.39, p < 0.001$)	Sill ($\beta = -0.28, p = 0.016$)
	Age + microstructure	OstAr ($\beta = 0.42, p < 0.001$)	
	Best combination	VasPor ($\beta = -0.28, p = 0.001$)	OstAr ($\beta = 0.34, p = 0.001$)
	Age + porosity		
	Age + heterogeneity		
	Age + microstructure		
	Best combination		

^a None of the interaction terms were significant.

^b β is the standardized coefficients from the general linear model.

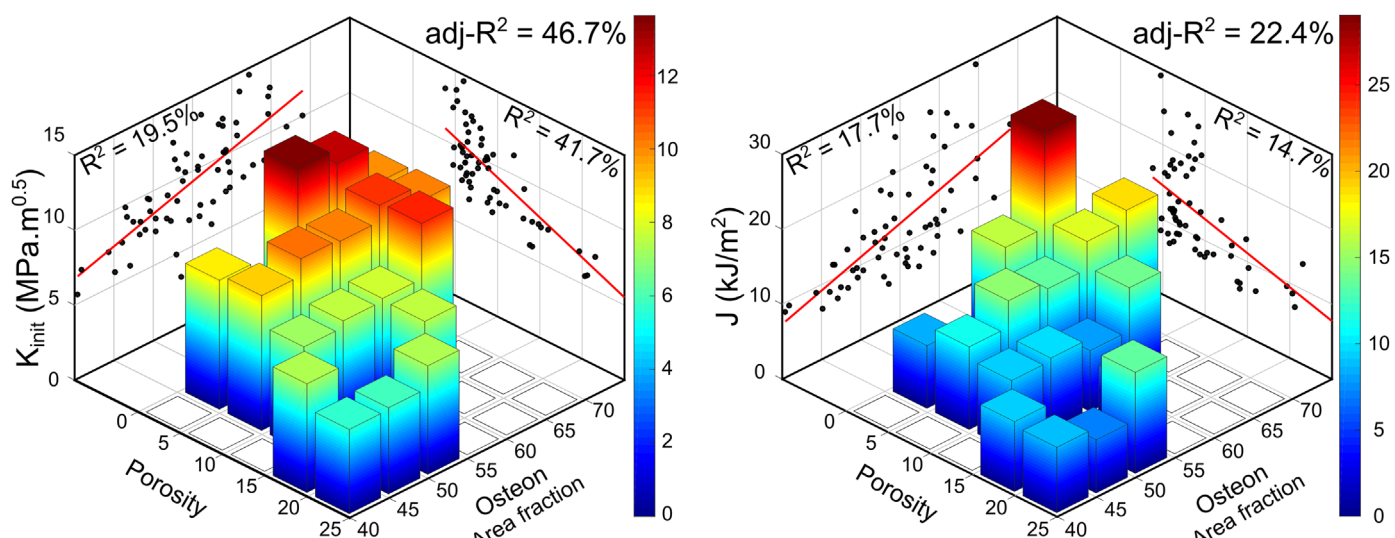


Fig. 5. 3D bar graphs representing fracture toughness properties (K_{init} on the left, J on the right) as a function of vascular porosity and osteonal area fraction. Simple linear regressions are plotted in the background for each variable.

variance in the fracture toughness properties (Table 2). Statistical significance of a predictor was reached when the associated p -value was less than 0.05. Analyses were performed using STATA 12 (StataCorp LP, College Station, TX).

3. Results

The vascular porosity estimated from qBEI images of a neighboring cross-section strongly correlated with the porosity of the material in the crack path as assessed with μ CT prior to mechanical testing ($R^2=87.2\%$). While the slope of the linear fit between VasPor and Ct.Po was not significantly different from unity, the intercept was significantly different from zero: qBEI yielded higher values of porosity compared to μ CT, possibly because of the lower resolution of the latter technique (Supplementary Fig. 4).

Among all reported parameters, vascular porosity showed the highest, negative correlation with crack initiation toughness (K_{init}) and the energy dissipated (J) during fracture (Table 1). As higher porosity was associated with more clustered pores (Supplementary Table 2), a more heterogeneous spatial distribution of porosity was also related to a decrease in the aforementioned

fracture toughness properties (Table 1). Lacunar porosity was positively correlated with fracture toughness properties (Table 1). However, this relationship may not be causal but rather reflects the fact that both lacunar porosity and fracture toughness properties decrease with age. Indeed, the correlations between lacunar porosity and fracture toughness properties were not significant when adding age as a covariate.

Among the parameters characterizing the distribution of mineralization within the matrix, the average degree of mineralization (BSEPeak), bulk or population heterogeneity in tissue mineralization (BSEwidth) and mineralization ratio between interstitial and osteonal tissue (IORatio) did not correlate with any of the fracture toughness properties (Table 1). However, local heterogeneity (sill) as derived from the variogram analysis was greater in bone specimens with a lower resistance to crack initiation (K_{init}) and a reduced ability to dissipate energy (J) (Table 1).

With respect to the microstructure, bone specimens having a greater area fraction of osteonal tissue (OstAr) tended to have greater resistance to crack initiation and propagation (Table 1 and Fig. 5). Microstructure, local heterogeneity in mineralization, and

vascular porosity each remained significant predictors of crack initiation toughness and energy dissipated during fracture after adjusting for age. Cortical porosity had a stronger contribution to K_{init} than age, whereas age had a stronger contribution to K_{init} than the heterogeneity parameters ($BSEwidth$ and $sill$) and $OstAr$ (standardized coefficients, Table 2). The combination that best explained the age-related variance in fracture toughness properties included age, cortical porosity, and the microstructural feature related to cement lines (Table 2 and Fig. 5). Most notably, none of the parameters describing the heterogeneity in mineralization ($BSEwidth$, $sill$ or $IOratio$) combined with either $VasPor$ or $OstAr$ improved the prediction of fracture toughness.

4. Discussion

Changes in the distribution of bone mineralization occurring with aging, disease, or treatment have prompted concerns that alterations in mineralization heterogeneity may affect the fracture resistance of bone. Owing to the multifactorial nature of toughening mechanisms occurring in bone, we aimed to put into perspective the relative contribution of heterogeneity in mineralization to bone fracture resistance in comparison to other important factors. Our results obtained from 62 human donors spanning the age of adulthood (21 years to 101 years) suggest that changes in porosity and microstructure overwhelm the contribution of heterogeneity in tissue mineralization to explain the age-related loss in fracture toughness of human cortical bone.

As expected from experimental (Yeni et al., 1997) and computational studies (Besdo and Vashishth, 2012; Tang and Vashishth, 2011; Ural and Vashishth, 2007), our data confirmed the detrimental effect of an increase in intracortical porosity on bone's fracture toughness: the matrix of highly porous tissue presents higher local strains, facilitating the initiation of cracks which then propagate faster through the pores. In addition, we found that a more clustered distribution of porosity was negatively correlated with the three fracture toughness properties of human cortical bone. However, because greater vascular porosity was associated with a more clustered distribution of pores ($r=0.86$, Supplemental Table 2), the pore clustering did not help improve the prediction of fracture toughness properties when accounting for intra-cortical porosity.

In addition to porosity, bone microstructure (i.e., the compartmentalization of the matrix in osteonal and interstitial tissue) possibly plays an important role in bone's ability to resist fracture as cement lines and lamellar pattern in osteons affect the propagation of cracks in bone tissue (Chan et al., 2009; Ural and Mischnicki, 2013; Ziopoulos, 2001). Our results suggest that an overall greater osteonal area fraction increases bone's fracture toughness properties, even when including the contribution of porosity. This suggests that the presence of relatively newer tissue within osteons and cement lines favor fracture resistance. Interestingly, $OstAr$ was the only selected property to correlate with crack propagation toughness supporting the importance of cement lines to crack deflection, but significance of this relationship was lost when age was included as covariate. Histological studies of human bone have shown that linear microcracks preferentially form and propagate within interstitial bone and are arrested by the cement lines and lamellar interfaces of osteons (Diab and Vashishth, 2007): this would explain why a greater osteonal area fraction favors bone's resistance to fracture.

Even though material heterogeneity is thought to promote toughening mechanisms in composites like bone, population and local heterogeneity in tissue mineralization were negatively correlated with crack initiation toughness and energy dissipated during fracture when age was included as covariate (Table 2); and

notably, a local measure ($sill$) was a better predictor than a bulk measure ($BSEwidth$) of heterogeneity. This is consistent with findings reporting weak, negative correlations between heterogeneity in microhardness (mean ratio of interstitial to osteonal areas) and fracture toughness in which the crack propagation was parallel to the osteonal axis (Phelps et al., 2000) or fatigue strength of cortical bone in tension (Ziopoulos et al., 2008) and supports the notion that heterogeneity at the length scale of ~200 μm can promote crack formation by concentrating strains within the bone matrix. Nonetheless, the prevailing finding of this work is that microstructural heterogeneity in tissue mineralization did not help explain changes in fracture toughness properties after accounting for age, porosity and microstructure. This is in agreement with the findings from the largest tissue composition study to date (Boskey et al., 2016) showing that heterogeneity in various outcomes (mineral-to-matrix ratio, carbonate-to-phosphate ratio, crystallinity, acid phosphate substitution, collagen maturity) at the micron length scale is not significantly different between female subjects with and without a fracture, when controlling for age and areal bone mineral density (60 subjects in each group).

The present study brings new insights into interpreting the effect of treatment-related changes at the tissue level on bone's fracture resistance. In particular, the association between the occurrence of a typical femoral fractures and the long-term use of bisphosphonates, established as the first-line therapy for osteoporosis, has promulgated the idea that the reduced microstructural heterogeneity in mineralization observed in treated patients (Donnelly et al., 2012; Roschger et al., 2008; Zoehler et al., 2006) may contribute to these rare, but adverse events (Ettinger et al., 2013). Our results suggest that the significant reduction in cortical porosity that follows anti-resorptive treatment (Borah et al., 2010; Misof et al., 2014; Zebaze et al., 2014) would far outweigh the shift toward a more homogenous tissue mineralization. Moreover, that shift back to a narrower distribution may itself promote fracture resistance as menopause-related increase in remodeling likely leads to excessive heterogeneity (Roschger et al., 2008), which could decrease crack initiation toughness (Table 2). Notably, bisphosphonates remain effective in reducing fracture risk for a vast majority of patients after years of use (Chen and Sambrook, 2012; Eriksen et al., 2014), though drug holidays may minimize the impact of suppressed remodeling on the accumulation of glycation-mediated, non-enzymatic crosslinks. Generally, the present study points out that difficulty in establishing a causal relationship between tissue mineralization and skeletal fragility if underlying changes in porosity are ignored.

This study is limited to a few features of cortical bone which only capture up to 50% of the variance in fracture toughness properties highlighting the need to investigate alternative toughening mechanisms to fully comprehend bone's fracture resistance. The favorable role of osteonal tissue (Table 2) likely pertains to its concentric lamellar structure where layers of mineralized collagen fibers are laid with changing orientations (Giraud-Guille, 1988), requiring more energy for a crack to penetrate through this composite structure. Indeed, the mechanical inhomogeneity at the lamellar scale produced by different collagen fiber orientation has been described as an important toughening mechanism (Katsamenis et al., 2015) in addition to the orientation of the collagen fibrils relative to the crack direction (Peterlik et al., 2006). This suggests that heterogeneity in collagen orientation rather than in tissue mineralization could be a more important determinant of bone fracture toughness. It remains to be seen whether alterations in collagen-related properties (e.g., crosslinking profile, amount of collagen) would significantly contribute to bone's integrity in addition to cortical porosity. The non-mineral component of the matrix may actually be a more important contributor to fracture toughness than mineralization as computational models suggest

that heterogeneity in plastic rather than elastic properties plays a major role in promoting energy dissipation at the sub-micron scale (Yao et al., 2011). Moreover, material heterogeneity at length scales smaller than a micron may promote fracture toughness of cortical bone as suggested by computational modeling (Tai et al., 2007). Finally, numerous mechanisms at the nanoscale also participate in providing bone its ability to resist fracture (Thurner and Katsamenis, 2014), including non-enzymatic collagen cross-links (Poundarik et al., 2015), non-collagenous proteins (Katsamenis et al., 2013; Poundarik et al., 2012), bound water (Granke et al., 2015), and microdamage (Norman et al., 1998; Seref-Ferlengez et al., 2015; Ziopoulos, 2001).

Another limitation of the present study was that specimens came from the femoral mid-shaft, which is not a typical fracture site. However, it is reasonable to assume that aging, diseases, or drug therapy would affect the skeleton in a systemic manner, in other words, changes in porosity and mineralization occurring at the femoral mid-shaft would also occur at the femoral neck. In a recent study, Abraham et al. (2015) showed that porosity, micro-indentation, and collagen crosslinks measures at the tibia could predict fragility of the femoral neck.

In summary, assessing the microstructure of cortical bone specimens from 62 human donors, we found that age, cortical porosity and osteonal fraction explained up to 50% of the variance in bone's fracture toughness properties and that including microstructural heterogeneity in tissue mineralization did not improve upon this prediction. Moreover, this heterogeneity is negatively correlated with crack initiation toughness. The findings of the present work stress the necessity to account for porosity and microstructure when evaluating the potential of matrix-related features to affect skeletal fragility.

Conflict of interest

The authors do not have a conflict of interest with present work.

Acknowledgments

The National Institute of Arthritis and Musculoskeletal and Skin Diseases of the National Institutes of Health (NIH) under AR063157 primarily funded this work. The micro-computed tomography scanner was supported by the National Center for Research Resources (1S10RR027631) and matching funds from the Vanderbilt Office of Research. Additional funding to perform the work was received from the Department of Veterans Affairs, Veterans Health Administration, Office of Research and Development (1I01BX001018) and the National Science Foundation (1068988) to collect specimens and develop the fracture toughness testing protocol. SEM imaging was performed through the use of the VUMC Cell Imaging Shared Resource (supported by NIH Grants CA68485, DK20593, DK58404, DK59637 and EY08126).

Appendix A. Supplementary material

Supplementary data associated with this article can be found in the online version at <http://dx.doi.org/10.1016/j.jbiomech.2016.06.009>.

References

- Abraham, A.C., Agarwalla, A., Yadavalli, A., McAndrew, C., Liu, J.Y., Tang, S.Y., 2015. multiscale predictors of femoral neck *in situ* strength in aging women: contributions of BMD, cortical porosity, reference point indentation, and nonenzymatic glycation. *J. Bone Miner. Res.* 30, 2207–2214.
- Ahmed, L.A., Shigdel, R., Joakimsen, R.M., Eldevik, O.P., Eriksen, E.F., Ghazem-Zadeh, A., Bala, Y., Zebaze, R., Seeman, E., Björnerem, A., 2015. Measurement of cortical porosity of the proximal femur improves identification of women with non-vertebral fragility fractures. *Osteoporos. Int.* 26, 2137–2146.
- ASTM Standard E1820-15a, 2015. Standard Test Method for Measurement of Fracture Toughness.
- Aurenhammer, F., 1991. Voronoi diagrams – a survey of a fundamental geometric data structure. *ACM Comput. Surv.* 23, 345–405.
- Bala, Y., Zebaze, R., Ghazem-Zadeh, A., Atkinson, E.J., Iuliano, S., Peterson, J.M., Amin, S., Björnerem, A., Melton 3rd, L.J., Johansson, H., Kanis, J.A., Khosla, S., Seeman, E., 2014. Cortical porosity identifies women with osteopenia at increased risk for forearm fractures. *J. Bone Miner. Res.* 29, 1356–1362.
- Bell, K.L., Loveridge, N., Jordan, G.R., Power, J., Constant, C.R., Reeve, J., 2000. A novel mechanism for induction of increased cortical porosity in cases of intracapsular hip fracture. *Bone* 27, 297–304.
- Bell, K.L., Loveridge, N., Power, J., Garrahan, N., Meggitt, B.F., Reeve, J., 1999. Regional differences in cortical porosity in the fractured femoral neck. *Bone* 24, 57–64.
- Bernhard, A., Milovanovic, P., Zimmermann, E.A., Hahn, M., Djonic, D., Krause, M., Breer, S., Puschel, K., Djuric, M., Amling, M., Busse, B., 2013. Micromorphological properties of osteons reveal changes in cortical bone stability during aging, osteoporosis, and bisphosphonate treatment in women. *Osteoporos. Int.* 24, 2671–2680.
- Besdo, S., Vashishth, D., 2012. Extended finite element models of intracortical porosity and heterogeneity in cortical bone. *Comput. Mater. Sci.* 64, 301–305.
- Bilger, N., Auslender, F., Bornert, M., Michel, J.-C., Moulinec, H., Suquet, P., Zaoui, A., 2005. Effect of a nonuniform distribution of voids on the plastic response of voided materials: a computational and statistical analysis. *Int. J. Solids Struct.* 42, 517–538.
- Borah, B., Dufresne, T., Nurre, J., Phipps, R., Chmielewski, P., Wagner, L., Lundy, M., Bouxsein, M., Zebaze, R., Seeman, E., 2010. Risedronate reduces intracortical porosity in women with osteoporosis. *J. Bone Miner. Res.* 25, 41–47.
- Boskey, A.L., Donnelly, E., Boskey, E., Spevak, L., Ma, Y., Zhang, W., Lappe, J., Recker, R.R., 2016. Examining the relationships between bone tissue composition, compositional heterogeneity and fragility fracture: a matched case controlled FTIR study. *J. Bone Miner. Res.* 31, 1070–1081.
- Bousson, V., Bergot, C., Wu, Y., Jolivet, E., Zhou, L.Q., Laredo, J.D., 2011. Greater tissue mineralization heterogeneity in femoral neck cortex from hip-fractured females than controls: a microradiographic study. *Bone* 48, 1252–1259.
- Chan, K.S., Chan, C.K., Nicolla, D.P., 2009. Relating crack-tip deformation to mineralization and fracture resistance in human femur cortical bone. *Bone* 45, 427–434.
- Chen, J.S., Sambrook, P.N., 2012. Antiresorptive therapies for osteoporosis: a clinical overview. *Nature reviews. Endocrinology* 8, 81–91.
- Diab, T., Vashishth, D., 2007. Morphology, localization and accumulation of *in vivo* microdamage in human cortical bone. *Bone* 40, 612–618.
- Dimas, L.S., Giesa, T., Buehler, M.J., 2014. Coupled continuum and discrete analysis of random heterogeneous materials: Elasticity and fracture. *J. Mech. Phys. Solids* 63, 481–490.
- Dong, X.N., Luo, Q., Sparkman, D.M., Millwater, H.R., Wang, X., 2010. Random field assessment of nanoscopic inhomogeneity of bone. *Bone* 47, 1080–1084.
- Dong, X.N., Pinninti, R., Lowe, T., Cussen, P., Ballard, J.E., Di Paolo, D., Shirvaikar, M., 2015. Random field assessment of inhomogeneous bone mineral density from DXA scans can enhance the differentiation between postmenopausal women with and without hip fractures. *J. Biomech.* 48, 1043–1051.
- Donnelly, E., Lane, J.M., Boskey, A.L., 2014. Research perspectives: the 2013 AAOS/ORS research symposium on bone quality and fracture prevention. *J. Orthop. Res.* 32, 855–864.
- Donnelly, E., Meredith, D.S., Nguyen, J.T., Gladnick, B.P., Rebollo, B.J., Shaffer, A.D., Lorich, D.G., Lane, J.M., Boskey, A.L., 2012. Reduced cortical bone compositional heterogeneity with bisphosphonate treatment in postmenopausal women with intertrochanteric and subtrochanteric fractures. *J. Bone Miner. Res.* 27, 672–678.
- Eriksen, E.F., Diez-Perez, A., Boonen, S., 2014. Update on long-term treatment with bisphosphonates for postmenopausal osteoporosis: a systematic review. *Bone* 58, 126–135.
- Ettinger, B., Burr, D.B., Ritchie, R.O., 2013. Proposed pathogenesis for atypical femoral fractures: lessons from materials research. *Bone* 55, 495–500.
- Giraud-Guille, M.M., 1988. Twisted plywood architecture of collagen fibrils in human compact bone osteons. *Calcif. Tissue Int.* 42, 167–180.
- Gourion-Arsiquaud, S., Lukashova, L., Power, J., Loveridge, N., Reeve, J., Boskey, A.L., 2013. Fourier transform infrared imaging of femoral neck bone: reduced heterogeneity of mineral-to-matrix and carbonate-to-phosphate and more variable crystallinity in treatment-naïve fracture cases compared with fracture-free controls. *J. Bone Miner. Res.* 28, 150–161.
- Granke, M., Makowski, A.J., Uppuganti, S., Does, M.D., Nyman, J.S., 2015. Identifying novel clinical surrogates to assess human bone fracture toughness. *J. Bone Miner. Res.* 30, 1290–1300.
- Hossain, M.Z., Hsueh, C.J., Bourdin, B., Bhattacharya, K., 2014. Effective toughness of heterogeneous media. *J. Mech. Phys. Solids* 71, 15–32.
- Jordan, G.R., Loveridge, N., Bell, K.L., Power, J., Rushton, N., Reeve, J., 2000. Spatial clustering of remodeling osteons in the femoral neck cortex: a cause of weakness in hip fracture? *Bone* 26, 305–313.
- Katsamenis, O.L., Chong, H.M., Andriotis, O.G., Thurner, P.J., 2013. Load-bearing in cortical bone microstructure: Selective stiffening and heterogeneous strain distribution at the lamellar level. *J. Mech. Behav. Biomed. Mater.* 17, 152–165.

- Katsamenis, O.L., Jenkins, T., Thurner, P.J., 2015. Toughness and damage susceptibility in human cortical bone is proportional to mechanical inhomogeneity at the osteonal-level. *Bone* 76, 158–168.
- Milovanovic, P., Rakocevic, Z., Djonic, D., Zivkovic, V., Hahn, M., Nikolic, S., Amling, M., Busse, B., Djuric, M., 2014. Nano-structural, compositional and micro-architectural signs of cortical bone fragility at the superolateral femoral neck in elderly hip fracture patients vs. healthy aged controls. *Exp. Gerontol.* 55, 19–28.
- Misof, B.M., Patsch, J.M., Roschger, P., Muschitz, C., Gamsjaeger, S., Paschalidis, E.P., Prokop, E., Klaushofer, K., Pietschmann, P., Resch, H., 2014. Intravenous treatment with ibandronate normalizes bone matrix mineralization and reduces cortical porosity after two years in male osteoporosis: a paired biopsy study. *J Bone Miner. Res.* 29, 440–449.
- Norman, T.L., Yeni, Y.N., Brown, C.U., Wang, Z., 1998. Influence of microdamage on fracture toughness of the human femur and tibia. *Bone* 23, 303–306.
- O'Brien, F.J., Taylor, D., Lee, T.C., 2003. Microcrack accumulation at different intervals during fatigue testing of compact bone. *J Biomech.* 36, 973–980.
- Otsu, N., 1979. A threshold selection method from gray-level histograms. *IEEE Trans. Syst., Man, Cybern.* 9, 62–66.
- Peterlik, H., Roschger, P., Klaushofer, K., Fratzl, P., 2006. From brittle to ductile fracture of bone. *Nat. Mater.* 5, 52–55.
- Phelps, J.B., Hubbard, G.B., Wang, X., Agrawal, C.M., 2000. Microstructural heterogeneity and the fracture toughness of bone. *J Biomed. Mater. Res.* 51, 735–741.
- Poundarik, A.A., Diab, T., Sroga, G.E., Ural, A., Boskey, A.L., Gundberg, C.M., Vashishth, D., 2012. Dilatational band formation in bone. *Proc. Natl. Acad. Sci. USA* 109, 19178–19183.
- Poundarik, A.A., Wu, P.C., Evis, Z., Sroga, G.E., Ural, A., Rubin, M., Vashishth, D., 2015. A direct role of collagen glycation in bone fracture. *J Mech. Behav. Biomed. Mater.* 50, 82–92.
- Roschger, P., Paschalidis, E.P., Fratzl, P., Klaushofer, K., 2008. Bone mineralization density distribution in health and disease. *Bone* 42, 456–466.
- Seref-Ferlemez, Z., Kennedy, O.D., Schaffler, M.B., 2015. Bone microdamage, remodeling and bone fragility: how much damage is too much damage? *Bonekey Rep.* 4, 644.
- Shigdel, R., Osima, M., Ahmed, L.A., Joakimsen, R.M., Eriksen, E.F., Zebaze, R., Björnerem, A., 2015. Bone turnover markers are associated with higher cortical porosity, thinner cortices, and larger size of the proximal femur and non-vertebral fractures. *Bone* 81, 1–6.
- Tai, K., Dao, M., Suresh, S., Palazoglu, A., Ortiz, C., 2007. Nanoscale heterogeneity promotes energy dissipation in bone. *Nat. Mater.* 6, 454–462.
- Tang, S.Y., Vashishth, D., 2011. The relative contributions of non-enzymatic glycation and cortical porosity on the fracture toughness of aging bone. *J Biomech.* 44, 330–336.
- Thurner, P.J., Katsamenis, O.L., 2014. The role of nanoscale toughening mechanisms in osteoporosis. *Curr. Osteoporos. Rep.* 12, 351–356.
- Tommasini, S.M., Nasser, P., Hu, B., Jepsen, K.J., 2008. Biological co-adaptation of morphological and composition traits contributes to mechanical functionality and skeletal fragility. *J Bone Miner. Res.* 23, 236–246.
- Ural, A., Mischnick, S., 2013. Multiscale modeling of bone fracture using cohesive finite elements. *Eng. Fract. Mech.* 103, 141–152.
- Ural, A., Vashishth, D., 2007. Effects of intracortical porosity on fracture toughness in aging human bone: a microCT-based cohesive finite element study. *J Biomed. Eng.* 129, 625–631.
- Ural, A., Vashishth, D., 2014. Hierarchical perspective of bone toughness – from molecules to fracture. *Int. Mater. Rev.* 59, 245–263.
- Wachter, N.J., Krischak, G.D., Mentzel, M., Sarkar, M.R., Ebinger, T., Kinzl, L., Claes, L., Augat, P., 2002. Correlation of bone mineral density with strength and micro-structural parameters of cortical bone in vitro. *Bone* 31, 90–95.
- Wang, M., Gao, X., Abdel-Wahab, A., Li, S., Zimmerman, E.A., Riedel, C., Busse, B., Silberschmidt, V., 2015. Effect of micromorphology of cortical bone tissue on crack propagation under dynamic loading. *EPJ Web Conf.* 94, 03005.
- Yao, H., Dao, M., Carnelli, D., Tai, K., Ortiz, C., 2011. Size-dependent heterogeneity benefits the mechanical performance of bone. *J Mech. Phys. Solids* 59, 64–74.
- Yeni, Y.N., Brown, C.U., Wang, Z., Norman, T.L., 1997. The influence of bone morphology on fracture toughness of the human femur and tibia. *Bone* 21, 453–459.
- Zebaze, R.M., Libanati, C., Austin, M., Ghasem-Zadeh, A., Hanley, D.A., Zanchetta, J.R., Thomas, T., Boutroy, S., Bogado, C.E., Bilezikian, J.P., Seeman, E., 2014. Differing effects of denosumab and alendronate on cortical and trabecular bone. *Bone* 59, 173–179.
- Zioupos, P., 2001. Accumulation of in-vivo fatigue microdamage and its relation to biomechanical properties in ageing human cortical bone. *J Microsc.* 201, 270–278.
- Zioupos, P., Gresle, M., Winwood, K., 2008. Fatigue strength of human cortical bone: age, physical, and material heterogeneity effects. *J Biomed. Mater. Res. A* 86, 627–636.
- Zoehler, R., Roschger, P., Paschalidis, E.P., Hofstaetter, J.G., Durchschlag, E., Fratzl, P., Phipps, R., Klaushofer, K., 2006. Effects of 3- and 5-year treatment with risendronate on bone mineralization density distribution in triple biopsies of the iliac crest in postmenopausal women. *J Bone Miner. Res.* 21, 1106–1112.